

See, Act, Adapt: Active Perception for Unsupervised Cross-Domain Visual Adaptation via Personalized VLM-Guided Agent

Tianci Tang¹ Tielong Cai¹ Hongwei Wang¹ Gaoang Wang¹

Abstract

Pre-trained perception models excel in generic image domains but degrade significantly in novel environments like indoor scenes. The conventional remedy is fine-tuning on downstream data which incurs catastrophic forgetting of prior knowledge and demands costly, scene-specific annotations. We propose a paradigm shift through Sea² (See, Act, Adapt): rather than adapting the perception modules themselves, we adapt how they are deployed through an intelligent pose-control agent. Sea² keeps all perception modules frozen, requiring no downstream labels during training, and uses only scalar perceptual feedback to navigate the agent toward informative viewpoints. Specially, we transform a vision-language model (VLM) into a low-level pose controller through a two-stage training pipeline: first fine-tuning it on rule-based exploration trajectories that systematically probe indoor scenes, and then refining the policy via unsupervised reinforcement learning that constructs rewards from the perception module’s outputs and confidence. Unlike prior active perception methods that couple exploration with specific models or collect data for retraining them, Sea² directly leverages off-the-shelf perception models for various tasks without the need for retraining. We conducted experiments on three visual perception tasks, including visual grounding, segmentation and 3D box estimation, with performance improvements of 13.54%, 15.92% and 27.68% respectively on dataset ReplicaCAD.

1. Introduction

Large-scale visual models pre-trained on internet-scale imagery have demonstrated remarkable generalization across recognition, segmentation, and visual grounding tasks (Xiao

¹Zhejiang University, Hangzhou, China. Correspondence to: Tianci Tang <tianci.24@intl.zju.edu.cn>, Gaoang Wang <gaoangwang@intl.zju.edu.cn>.

Preprint. March 2, 2026.

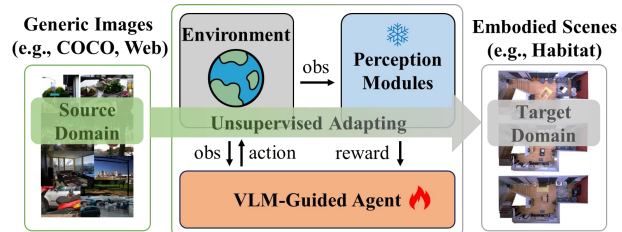


Figure 1. Overview of unsupervised cross-domain adaptation via VLM-guided active perception agent. (Left) Source domain including generic images (e.g., COCO (Lin et al., 2015), Web) where perception models pre-trained on. (Middle) Our embodied agent actively explores the indoor environment and adjusts its camera pose to capture information-rich observations that maximize perception quality. (Right) Target domain including embodied scenes (e.g., Habitat (Savva et al., 2019)) where our VLM-guided agent trained on to unsupervised adapt the domain gap.

et al., 2024; 2023; Ravi et al., 2024; Ren et al., 2024; He et al., 2021; Cheng et al., 2024). However, when deployed in novel embodied environments such as indoor scenes, their performance degrades sharply due to domain gaps in viewpoint distribution, occlusion patterns, and spatial semantics (Yang et al., 2019; Ammirato et al., 2017; Zeng et al., 2020; Fan et al., 2024). The prevailing remedy is fine-tuning perception modules on downstream data, while it incurs two critical limitations: catastrophic forgetting of prior knowledge and the prohibitive cost of acquiring scene-specific annotations (e.g., pixel masks, 3D bounding boxes, or referring expressions). This raises a fundamental question: *Can we adapt perception to new domains without touching the models themselves?*

We propose a paradigm shift: instead of adapting perception modules themselves, we adapt how they are deployed. Our key insight is that perceptual performance depends not only on model capacity but also critically on the informativeness of the observation viewpoint (Yang et al., 2019; Fan et al., 2024). By intelligently controlling the agent’s pose to seek out informative views, we can recover performance drops without retraining, annotating data, or modifying the perception system. Crucially, our approach freezes all perception modules, requiring no downstream labels during agent training; it relies solely on scalar feedback derived directly from the frozen perception module (e.g., detection confidence,



Figure 2. **Illustration of the active perception process for segmentation.** The agent decomposes the instruction into task-specific metadata and reasons about the scene to execute camera-adjusting actions. Starting from a highly occluded initial view (yellow) where the perception output (green mask) for the target object (red box) is poor, it follows a trajectory of navigational steps (blue) to reduce visual ambiguity. The final viewpoint (red) offers a significantly clearer perspective for the perception module, yielding a substantial improvement in perception score compared to the initial state.

segmentation quality, or 3D consistency). This enables operation in open-world settings where ground-truth annotations are unavailable, unlike prior active perception methods that either tightly couple exploration with specific architectures (Chaplot et al., 2021; Kotar & Mottaghi, 2022; Ding et al., 2023) or collect labeled data for retraining (Scarpellini et al., 2024; Jing & Kong, 2023). Moreover, unlike recent RL-based approaches that assume closed-set tasks or rely on task-specific uncertainty models (Ding et al., 2023; Fan et al., 2024), our framework leverages semantic reasoning to handle open-ended, natural-language-driven objectives (e.g., “Locate the bicycle next to the door.”) while generalizing across diverse perception backbones.

To realize this vision, we transform a vision-language model (VLM) into a low-level pose controller through a two-stage training pipeline. First, we align the VLM with spatial reasoning via supervised fine-tuning on rule-based exploration trajectories that systematically probe indoor environments. Second, we refine the policy using unsupervised reinforcement learning (RL), where rewards are constructed from the outputs of the frozen perception module without access to any downstream perceptual annotations (e.g., ground-truth masks or bounding boxes). This decouples perception from control, creating a modular framework that seamlessly accommodates diverse off-the-shelf perception architectures without the need for task-specific retraining.

We validate our approach on three mainstream vision tasks on datasets ReplicaCAD (Szot et al., 2021) and HM3D (Ramakrishnan et al., 2021) in photo-realistic Habitat (Savva et al., 2019) including: visual grounding, segmentation, and 3D bounding box estimation. Sea² improves performance on ReplicaCAD and HM3D by 13.54%, 15.92%, and 27.68% and 22.16%, 12.49%, and 9.31%, respectively, demonstrating that strategic viewpoint selection can recover

domain-gap-induced degradation without a single annotated label. This establishes a new direction for label-efficient domain adaptation in embodied AI.

Our contributions can be summarized as follows:

- We present the first VLM-based active perception framework that achieves plug-and-play compatibility with diverse off-the-shelf models. By using only scalar outputs as rewards, Sea² enables seamless integration across various perception architectures without requiring retraining or downstream labels.
- We introduce an unsupervised RL training pipeline based on perception-derived rewards. By leveraging only task-level objectives and scalar outputs from frozen models, our method eliminates the need for dense perceptual annotations (e.g., pixel-level masks or 3D boxes), enabling effective policy learning in annotation-scarce environments.
- We demonstrate substantial gains across three visual tasks, including detection, segmentation, and 3D understanding, with improvements of 13.54%, 15.92%, and 27.68% in metrics on dataset ReplicaCAD, showing that viewpoint adaptation alone can effectively bridge domain gaps.

2. Related Work

2.1. Embodied Active Perception

Active perception studies how agents move to acquire views that improve recognition under occlusion and partial visibility. Early *Embodied Visual Recognition (EVR)* work showed that learned motion policies can outperform passive baselines for classification, amodal localization, and

segmentation in 3D environments (Yang et al., 2019). Subsequent lines either adapt the detector in-the-loop during interaction (Kotar & Mottaghi, 2022), or keep perception frozen and optimize the *policy* to seek informative views, e.g., decision-transformer control with offline+online training (Ding et al., 2023). Complementary efforts collect/evaluate informative multi-view data for self-training or exploration-aware adaptation (Fang et al., 2020; Chaplot et al., 2021; Jing & Kong, 2023; Scarpellini et al., 2024), incorporate uncertainty to guide viewpoint selection (Fan et al., 2024), extend from detection to active localization (Di Giammarino et al., 2024), and address embodied domain adaptation under distribution shift (Shi et al., 2025). Our work (i) keeps all perception modules *frozen* to avoid catastrophic forgetting, (ii) uses a single VLM policy that conditions on both images and natural-language task prompts to *control viewpoints* across multiple modules.

2.2. Multimodal Foundation Models

Multimodal foundation models provide open-vocabulary recognition and promptable perception. CLIP (Radford et al., 2021) aligns images and text for robust zero-shot recognition; BLIP-2 (Li et al., 2023) bridges frozen vision encoders and LLMs for efficient multimodal reasoning; Flamingo scales few-shot VLMs; instruction-tuned MLLMs such as LLaVA (Liu et al., 2023) improve visual instruction following. Recent families (Qwen3-VL (Yang et al., 2025), InternVL3.5 (Wang et al., 2025)) further enhance grounding and OCR across parameter scales. Recent work has utilized the multimodal perception and planning capabilities of VLM for embodied navigation (Zhang et al., 2024b;a; Jiang et al., 2025; Ao et al., 2025; Yin et al., 2024; Zhang et al., 2025) rather than purely for perception or generation. Inspired by this, we *use a VLM as an action policy* to translate language-grounded spatial reasoning into low-level control while keeping task modules frozen.

2.3. RL-based Post-training for VLMs

RLHF learns a reward model from human preferences, then optimize the policy with PPO under a KL constraint (InstructGPT) (Ouyang et al., 2022); strong alignment but costly and reward-sensitive. DPO removes reward modeling and directly fit a preference objective from pairs (Rafailov et al., 2023); simpler but still preference-dependent. GRPO-style objectives have recently improved long-horizon reasoning and training stability (Shao et al., 2024; Zheng et al., 2025; Yu et al., 2025). We adopt GRPO to train the VLM as an action policy from *unsupervised* rewards avoiding preference data and detector fine-tuning while enabling transferable, language-guided active perception.

3. Method

Our core premise is that perceptual performance degradation in novel domains stems not only from model capacity limitations, but also from suboptimal viewpoint selection (Yang et al., 2019; Fan et al., 2024). Rather than adapting perception modules, which risks catastrophic forgetting and demands costly annotations, we freeze all perception models and instead learn an unsupervised pose-control policy that navigates toward informative observations. The policy is optimized solely through scalar feedback from the frozen modules (confidence scores and geometric consistency), requiring no downstream labels during training. In this section, we introduce our framework design, which is an indoor VLM-guided embodied agent with three perception modules. We also elaborate on a two-stage training pipeline for our proposed method.

3.1. Overview and Problem Formulation

We formulate the task as an unsupervised active perception problem where an embodied agent controls its camera pose to maximize the quality of observations for a set of frozen perception modules \mathcal{M} . At episode onset, the agent receives a natural-language task instruction I and an initial observation o_1 . The agent’s policy π_θ generates the task prompt p , selects the perception module $m \in \mathcal{M}$ and outputs discrete actions $a_t \in \mathcal{A}$ over a horizon T to adjust its viewpoint, where \mathcal{A} includes translational and rotational movements (e.g., move forward, turn right/left, look up/down, stop).

The observation o_t at time t is an RGB image captured from the current pose. The frozen selected perception module m processes (o_t, p) to produce a prediction \hat{y}_t^m and a scalar confidence score $c_t^m \in [0, 1]$ indicating result reliability. Critically, no ground-truth labels are available for \hat{y}_t^m ; the agent must infer viewpoint quality solely from the sequence of (\hat{y}_t^m, c_t^m) .

Optimization Objective. The agent’s goal is to learn a policy π_θ that maximizes the cumulative quality of perception outcomes without updating any module parameters:

$$\max_{\theta} \mathbb{E}_{\pi_{\theta}} \left[\sum_{t=1}^T r(\{\hat{y}_t^m, c_t^m\}_{m \in \mathcal{M}}, o_t) \right] \quad (1)$$

where the reward $r(\cdot)$ is an unsupervised scalar signal derived entirely from the frozen modules’ outputs and geometric consistency checks. This decouples perception from control, enabling zero-shot transfer across module architectures and scenes.

3.2. Framework Design

Sea² employs a VLM as the action policy π_θ . The VLM receives a task instruction I (encoding the original task type

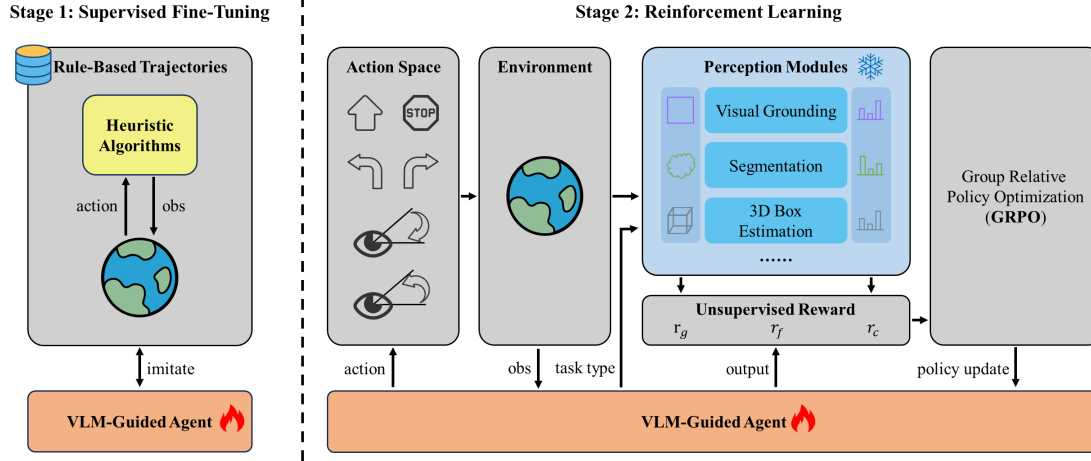


Figure 3. Illustration of our Sea² framework. In Stage 1, the VLM is fine-tuned on rule-based trajectories generated by heuristic algorithms to align it with spatial reasoning and control formats. In Stage 2, the VLM serves as a low-level pose controller for the agent, where it is further refined using unsupervised reinforcement learning with GRPO. The agent interacts with the environment, receiving observations and taking actions to optimize its policy based on rewards derived from the frozen selected perception module’s confidence and results (e.g., grounding confidence, mask area). The selected perception module remain frozen throughout the training process, ensuring no catastrophic forgetting of prior knowledge. The final policy enables the agent to navigate to informative viewpoints that enhance the performance of the perception modules without requiring any downstream annotations.

h_I and language description p_I of the target object, further details regarding the formulation of I are provided in the **Task Definition** (see 4.1.) and the current observation o_t , then generates a structured output comprising:

- **Thoughts:** A textual reasoning trace explaining the spatial reasoning (e.g., object location, occlusion assessment).
- **Task type:** A task routing result h used to select perception module $m \in \mathcal{M}$.
- **Task prompt:** A language description p of the task for the selected perception module m .
- **Action:** A discrete control command $a_t \in \mathcal{A}$.

The VLM is transformed from a passive reasoning model into an embodied pose controller through our two-stage training pipeline, *i.e.*, supervised fine-tuning (SFT) followed by reinforcement learning (RL).

Perception Module Interface. Each module $m \in \mathcal{M}$ implements a unified interface: given (o_t, p) , it returns a prediction \hat{y}_t^m (e.g., grounded 2D box, segmentation mask, or 3D box) and a confidence score c_t^m . The confidence is based on each perception module. During both SFT and RL, all modules remain frozen, treating them as black-box experts that provide feedback without adaptation.

3.3. Training Pipeline

As shown in Figure 3, the first stage involves supervised fine-tuning (SFT) of the VLM using rule-based trajectories. The second stage employs reinforcement learning (RL) with reward signals derived from perception modules’ feedback.

3.3.1. SUPERVISED FINE-TUNING (SFT)

To initialize the VLM with basic spatial reasoning and reduce RL exploration variance, we collect trajectories using a deterministic heuristic policy. The heuristic follows a three-phase logic:

- **Object Search:** Rotate until the target object is detected with non-zero confidence.
- **Viewpoint Centering:** Adjust the viewpoint to align the object’s predicted region with the image center.
- **Proximity Adjustment:** Move forward until the object occupies a sufficient image area, then stop.

Each trajectory records the heuristic’s “thoughts” (spatial reasoning), task type, task prompt and actions, forming a supervised dataset for SFT that aligns the VLM’s output format with embodied control requirements.

3.3.2. REINFORCEMENT LEARNING (RL)

After acquiring fundamental embodied perception skills through SFT, we further improve the model via reinforcement learning (RL) using perception-based reward signals.

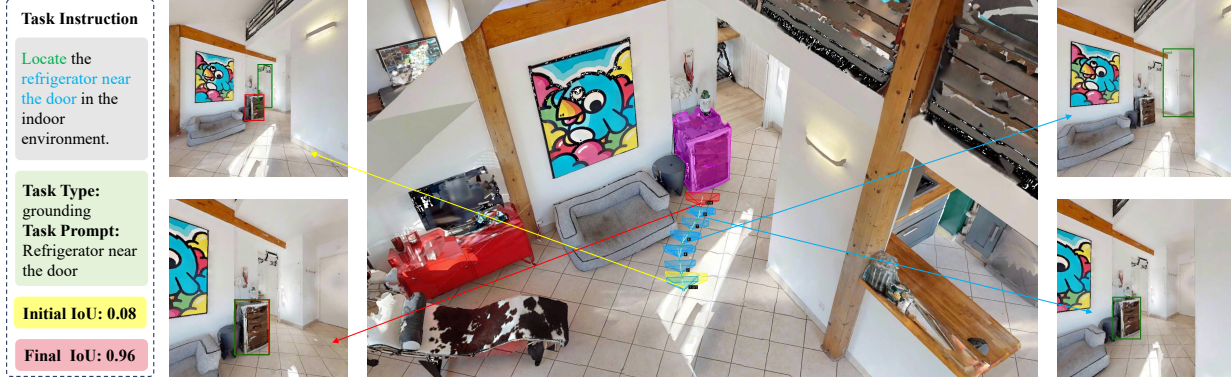


Figure 4. Illustration of the active perception process for visual grounding. From a poor initial view (yellow) where the prediction (green box) for the target (red box) is inaccurate, the agent takes navigational steps (blue) to reduce ambiguity, reaching a final viewpoint (red) that greatly improves the perception result.



Figure 5. Illustration of the active perception process for segmentation. From a poor initial view (yellow) where the prediction (green box) for the target (red box) is inaccurate, the agent takes navigational steps (blue) to reduce ambiguity, reaching a final viewpoint (red) that greatly improves the perception result.

In this stage, we adopt the Group Relative Policy Optimization (GRPO) algorithm and design a comprehensive reward function to guide policy optimization. The total reward is composed of a *format reward* r_f , a *confidence reward* r_c , and a *geometric reward* r_g . Among them, r_f is derived from the action policy output, while r_c and r_g are computed from the perception module outputs. The overall reward function is defined as:

$$r = \begin{cases} r_f + \lambda_1 r_c + \lambda_2 r_g, & \text{if } h = h_I \\ -1, & \text{if } h \neq h_I \end{cases} \quad (2)$$

where h and h_I denote the predicted and ground-truth task types, respectively. The agent receives a constant penalty of -1 for incorrect task identification; otherwise, the reward is defined as a weighted combination of the fundamental perception score r_f , the confidence score r_c , and the geometric consistency r_g . λ_1 and λ_2 weight the respective rewards and satisfy $\lambda_1 + \lambda_2 = 1$. Specifically, while the agent utilizes the ground-truth task type h_I to determine the reward structure, the training process remains entirely

independent of perceptual ground-truth annotations. This ensures that the policy learns to optimize observation quality using only the intrinsic feedback of the frozen perception models, making it applicable to open-world scenarios where precise spatial or semantic labels are unavailable.

Format Reward. The format reward r_f evaluates whether the model’s output structure adheres to the expected schema. Specifically, the reasoning process must be contained in the "thoughts": {} field, the action decision must appear in the "action": {} field, and only one action can be generated per step. This reward encourages the model to output well-structured and consistent reasoning–action pairs:

$$r_f = \begin{cases} 0.05, & \text{if the format is correct,} \\ -0.05, & \text{if the format is incorrect.} \end{cases} \quad (3)$$

Confidence Reward. The confidence reward r_c measures the change in the perception module’s confidence score between consecutive steps, encouraging the agent to increase confidence in its perception results without relying on ex-

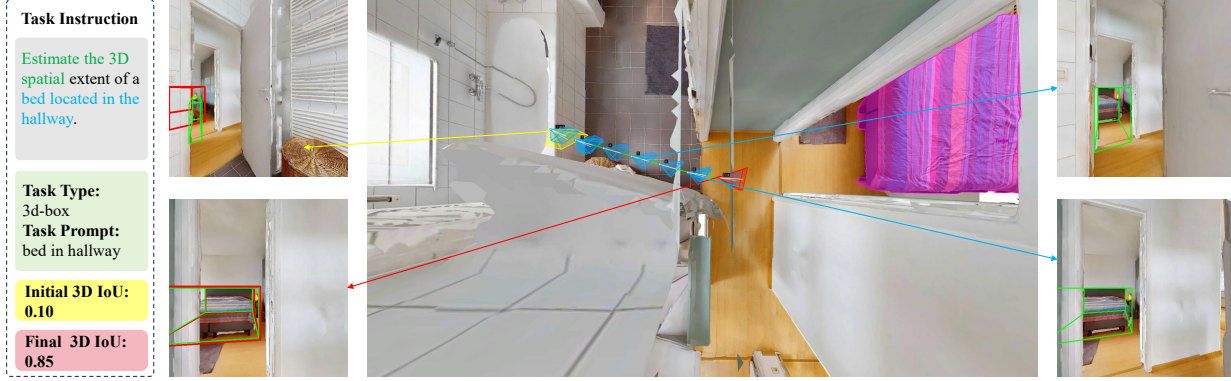


Figure 6. Illustration of the active perception process for 3D box estimation. From a poor initial view (yellow) where the prediction (green box) for the target (red box) is inaccurate, the agent takes navigational steps (blue) to reduce ambiguity, reaching a final viewpoint (red) that greatly improves the perception result.

ternal supervision. For visual grounding, the confidence is obtained from GroundingDINO; for segmentation, it is a weighted combination of GroundingDINO and SAM; and for 3D box estimation, it integrates confidence from GroundingDINO, SAM, and the 3D box estimator.

$$r_c = c_t^m - c_{t-1}^m \quad (4)$$

Geometric Reward. The geometric reward r_g enforces spatial consistency between the predicted region and the observation. It consists of two components: *area* and *center*.

The area reward measures the proportion of the predicted region \hat{y}_t^m within the current observation o_t , encouraging the model to approach the target object. For visual grounding, this ratio corresponds to the bounding-box area relative to the image; for segmentation, to the mask area; and for 3D box estimation, to the projected 3D box area.

$$r_a = \frac{A(\hat{y}_t^m)}{A(o_t)} \quad (5)$$

where $A(\cdot)$ is the area function.

The center reward encourages the model to align the predicted target region with the image center. Instead of using raw Euclidean distance, we compute a normalized alignment score between 0 and 1, where higher values indicate better alignment. This design stabilizes localization behavior and prevents excessive deviation from the target region during training.

$$r_u = 1 - d(u(\hat{y}_t^m), u(o_t)) \quad (6)$$

where $u(\cdot)$ extracts the predicted and observed center coordinates and $d(\cdot, \cdot)$ computes normalized distance.

The geometric reward r_g calculation method is as follows:

$$r_g = g_t^m - g_{t-1}^m \quad (7)$$

$$g_t^m = \mu_1 r_a + \mu_2 r_u \quad (8)$$

where g_t^m is the geometric score and μ_1 and μ_2 are the weights of individual rewards.

4. Experiments

4.1. Experimental Setup and Data

Task Definition. At the beginning of each episode, the agent is spawned at a random navigable pose with a forward-facing RGB camera (height 1 m, 512×512 resolution). We select as target an object that is (partially) in view and exceeds a minimum visible-area threshold to avoid degenerate language references. The task instruction I is synthesized via a two-stage hierarchical process. First, we employ Qwen2.5-VL-7B (Bai et al., 2025) to generate an open-vocabulary, attribute-aware language description p_I of the target object. Subsequently, the final task instruction I is formulated by conditioning on the ground-truth task type h_I (e.g., “segment the $[p_I]$ ”), thereby encoding both the target’s semantic attributes and the specific perceptual objective. The policy is allowed up to $T = 10$ steps and may issue `stop` early once it believes the current viewpoint is informative. Formally, given observation o_t and prompt p , the VLM-based policy π chooses an action $a_t = \pi(o_t, p)$ and we record the perception output sequence (\hat{y}^m, c^m) for each frozen module $m \in \mathcal{M}$.

Environments and Splits. All experiments are conducted in Habitat (Savva et al., 2019) on ReplicaCAD (Szot et al., 2021) suite (84 indoor scenes) and HM3D (Ramakrishnan et al., 2021) suite. For each suite, we randomly select 10 scenes for training and sample 500 tasks from the 10 training scenes to construct the test sets for evaluation.

Action Space and Observations. We use a low-level discrete action set with step sizes of 0.25 m (translation) and 10° (yaw/pitch). Vertical look controls are included to handle tall/near objects and reduce self-occlusion. Each step

Table 1. Three perception module baselines on ReplicaCAD with different controllers. Visual grounding is evaluated by mAP, segmentation by IoU and Dice, and 3D box estimation by IoU and Center Score (higher is better). The best results are highlighted in bold. Degraded results are highlighted in red, while improved results are highlighted in green. **Notably, the Shortest Path baseline is a ground-truth-informed (oracle) method: it possesses perfect prior knowledge of target locations, retrieving precise 3D coordinates from scene annotations and computing the shortest navigable path using the Habitat pathfinder.**

Perception Module + Policy	Visual Grounding			Segmentation		3D Box Estimation	
	mAP@0.5 ↑	mAP@0.75 ↑	mAP _{avg} ↑	IoU ↑	Dice ↑	IoU ↑	Center Score ↑
Pretrained Perception Module (PPM)	0.7958	0.6225	0.7092	0.5621	0.6398	0.2648	0.5499
PPM + Forward	0.4667	0.3897	0.4282	0.3495	0.3911	0.1503	0.3206
	(-41.37%)	(-37.40%)	(-39.62%)	(-37.82%)	(-38.87%)	(-43.24%)	(-41.70%)
PPM + Random	0.6662	0.5183	0.5923	0.4626	0.5282	0.2237	0.4809
	(-16.29%)	(-16.74%)	(-16.48%)	(-17.70%)	(-17.44%)	(-15.48%)	(-12.55%)
PPM + Heuristic	0.6969	0.5698	0.6334	0.5200	0.5849	0.2543	0.5310
	(-12.43%)	(-8.47%)	(-10.69%)	(-7.49%)	(-8.58%)	(-3.93%)	(-3.44%)
PPM + Shortest Path	0.8668	0.7198	0.7933	0.6075	0.6817	0.3259	0.6373
	(+8.92%)	(+15.64%)	(+11.86%)	(+8.07%)	(+6.55%)	(+23.09%)	(+15.89%)
PPM + InternVL3.5-2B	0.7020	0.5747	0.6384	0.5556	0.6322	0.2528	0.5250
	(-11.79%)	(-7.68%)	(-9.99%)	(-1.16%)	(-1.19%)	(-4.53%)	(-4.52%)
PPM + Qwen3VL-2B	0.6133	0.5097	0.5615	0.4214	0.4744	0.1781	0.4038
	(-22.93%)	(-18.13%)	(-20.83%)	(-25.03%)	(-25.85%)	(-32.74%)	(-26.57%)
PPM + Ours (InternVL3.5-2B)	0.8627	0.7055	0.7841	0.6251	0.7002	0.3195	0.6600
	(+8.40%)	(+13.33%)	(+10.56%)	(+11.21%)	(+9.44%)	(+20.67%)	(+20.03%)
PPM + Ours (Qwen3VL-2B)	0.8725	0.7378	0.8052	0.6516	0.7267	0.3380	0.6893
	(+9.63%)	(+18.53%)	(+13.54%)	(+15.92%)	(+13.59%)	(+27.68%)	(+25.35%)

provides the current RGB frame; depth is used only by the 3D module (below), not as an input channel to the policy.

Perception Modules. We consider three representative perception tasks and their modules $\mathcal{M}=\{\text{Visual Grounding, Segmentation, 3D Box Estimation}\}$; each returns a prediction and a scalar confidence $conf_m$ used for feedback and rewards. (i) *Visual Grounding* (VG) uses GroundingDINO (Liu et al., 2024) (GDINO) to produce a 2D bounding box and confidence (\hat{y}^{vg}, c^{vg}) given the language description and the current RGB frame. (ii) *Segmentation* first applies GroundingDINO to obtain a box and then SAM (Kirillov et al., 2023) to produce a mask (\hat{y}^{seg}) . Its confidence is a weighted combination of detector and mask confidences $c^{seg}=\mu_3c^{seg1}+\mu_4c^{seg2}$ (fixed weights across experiments). (iii) *3D Box Estimation* computes a point cloud by intersecting the mask with the depth image and fits an oriented 3D bounding box via minimum-area footprint search on the ground plane. Its confidence aggregates detector, mask, and geometric signals (e.g., point count, filtering retention, depth consistency) into $c^{3D} \in [0, 1]$.

SFT Data Collection. To align the pretrained VLM with embodied control and reduce RL exploration burden, we collect supervised trajectories with a deterministic heuristic that is agnostic to perception architectures: *Search*—rotate until the target becomes visible; *Centering*—partition the image into a 3×3 grid; if the target center is off-axis, issue $\{\text{turn_left, turn_right, look_up, look_down}\}$ to re-center; *Approach/Stop*—once centered, if the visible

region is below a threshold, `move_forward`; otherwise `stop`. At each step we log the textual "thoughts" and the "action" token. These trajectories seed the *SFT* stage.

GRPO Training Details. For reinforcement learning, we optimize the policy with GRPO using the following hyperparameters: initial learning rate 1×10^{-6} , 4 rollouts per update, batch size 8, KL coefficient 0.04, and sampling temperature 0.4. Rewards are computed from frozen-module feedback as defined in Equation (2) (confidence change in Equation (4) and geometric shaping in Equation (6)).

Baselines and Metrics. We compare against: (a) *Pretrained Perception Module (PPM)*—evaluate each frozen module on the first frame at $t=1$ (no action); (b) *Forward*—always execute `move_forward`; (c) *Random*—sample a random action from \mathcal{A} at each step; (d) *Heuristic*—the search-centering-approach heuristic used for SFT data collection; (e) *Shortest Path*—a baseline that has access to ground-truth object positions, serving as a reference for evaluating learned policies under the same constraints.

For baselines (a)–(e), the ground-truth task type h_I and target description p_I are directly provided as inputs. In contrast, for (f) *InternVL3.5-2B* (Wang et al., 2025) & *Qwen3VL-2B* (Yang et al., 2025) (prompt-based VLM controllers) and (g) *Ours (InternVL3.5)* & *Ours (Qwen3VL)* (trained via our two-stage pipeline), the models receive only the natural language instruction I . These models must autonomously parse the task type h and object description p from I . To

Table 2. Three perception module baselines on HM3D with different controllers. Visual grounding is evaluated by mAP, segmentation by IoU and Dice, and 3D box estimation by IoU and Center Score (higher is better). The best results are highlighted in **bold**. Degraded results are highlighted in red, while improved results are highlighted in green.

Perception Module + Policy	Visual Grounding			Segmentation		3D Box Estimation	
	mAP@0.5 ↑	mAP@0.75 ↑	mAP _{avg} ↑	IoU ↑	Dice ↑	IoU ↑	Center Score ↑
Pretrained Perception Module (PPM)	0.5914	0.4224	0.5069	0.4694	0.5460	0.3136	0.5653
PPM + Forward	0.3133	0.2475	0.2804	0.2362	0.2700	0.1429	0.2879
	(-47.02%)	(-41.40%)	(-44.68%)	(-49.69%)	(-50.55%)	(-54.42%)	(-49.08%)
PPM + Random	0.5032	0.3739	0.4386	0.4052	0.4689	0.2714	0.4866
	(-14.91%)	(-11.48%)	(-13.48%)	(-13.68%)	(-14.12%)	(-13.45%)	(-13.92%)
PPM + Heuristic	0.5403	0.4043	0.4723	0.4754	0.5384	0.3343	0.5700
	(-8.64%)	(-4.28%)	(-6.83%)	(+1.26%)	(-1.39%)	(+6.60%)	(+0.83%)
PPM + Shortest Path	0.5997	0.4988	0.5493	0.4915	0.5614	0.3316	0.5853
	(+1.40%)	(+18.09%)	(+8.35%)	(+4.71%)	(+2.82%)	(+5.74%)	(+3.53%)
PPM + InternVL3.5-2B	0.4512	0.3606	0.4059	0.4745	0.5526	0.3028	0.5482
	(-23.71%)	(-14.62%)	(-19.93%)	(+1.09%)	(+1.21%)	(-3.43%)	(-3.03%)
PPM + Qwen3VL-2B	0.4512	0.3606	0.4059	0.4326	0.5007	0.2761	0.4725
	(-23.71%)	(-14.62%)	(-19.93%)	(-7.85%)	(-8.29%)	(-11.95%)	(-16.42%)
PPM + Ours (InternVL3.5-2B)	0.6400	0.5230	0.5815	0.4981	0.5624	0.3306	0.5748
	(+8.21%)	(+23.82%)	(+14.72%)	(+6.12%)	(+3.01%)	(+5.42%)	(+1.67%)
PPM + Ours (Qwen3VL-2B)	0.6752	0.5633	0.6193	0.5261	0.5908	0.3420	0.5955
	(+14.17%)	(+33.37%)	(+22.16%)	(+12.49%)	(+8.57%)	(+9.31%)	(+5.67%)

Table 3. Ablation study on training strategies. Visual grounding is evaluated by mAP, segmentation by IoU and Dice, and 3D box estimation by IoU and Center Score (higher is better). The best results are highlighted in **bold**. Degraded results are highlighted in red, while improved results are highlighted in green.

Method	Visual Grounding			Segmentation		3D Box Estimation	
	mAP@0.5 ↑	mAP@0.75 ↑	mAP _{avg} ↑	IoU ↑	Dice ↑	IoU ↑	Center Score ↑
Pretrained Perception Module	0.7958	0.6225	0.7092	0.5621	0.6398	0.2648	0.5499
RL-Only	0.4647	0.3877	0.4262	0.3513	0.3921	0.1511	0.3239
	(-41.61%)	(-37.72%)	(-39.90%)	(-37.50%)	(-38.71%)	(-42.92%)	(-41.09%)
SFT-Only	0.8027	0.6738	0.7383	0.5997	0.6719	0.3099	0.6012
	(+0.86%)	(+8.25%)	(+4.10%)	(+6.70%)	(+5.02%)	(+17.05%)	(+9.32%)
SFT+RL	0.8627	0.7055	0.7841	0.6251	0.7002	0.3195	0.6600
	(+8.40%)	(+13.33%)	(+10.56%)	(+11.21%)	(+9.44%)	(+20.67%)	(+20.03%)

ensure rigorous evaluation, if a model misidentifies the task type ($h \neq h_I$), the corresponding metric for that episode is set to zero; furthermore, any distortion in the extracted p naturally impacts the downstream perception module’s performance.

We use AP for visual grounding, IoU/Dice for segmentation, and IoU/center score for 3D box estimation. Metrics are computed from the final module outputs at `stop` (or $t=T$). Baselines and metrics correspond to Table 1.

4.2. Performance in Perception Tasks

Following the setup and baselines defined in Section 4.1, Table 1 summarizes results on ReplicaCAD across visual grounding, segmentation, and 3D box estimation with frozen modules. Relative to the PPM baseline, our policy boosts VG AP_{avg} +13.54%, segmentation IoU +15.92% with Dice rising +13.59%, and 3D box IoU +27.68%, 3D center score +25.35%.

Simple motion baselines are ineffective or even harmful. `Forward` policy substantially degrades all metrics (e.g., -41.37% seg IoU), likely due to over-approaching that increases occlusion or truncation. `Random` motion is also inferior across tasks, underscoring that *which* view to acquire matters.

The `Heuristic` baseline improves segmentation and 3D box metrics only marginally (e.g., +3.37% seg IoU) and lags significantly behind our policy. This is primarily because `Heuristic` is purely reactive, relying entirely on the immediate feedback of the frozen perception module; consequently, any initial misdetection becomes unrecoverable, leading the agent into erroneous trajectories. Meanwhile, although `Shortest path` possesses privileged knowledge of the target’s 3D coordinates to ensure geometric reachability, its performance gains remain modest (e.g., +6.27% 3D IoU). This indicates that simply arriving at the target’s location is insufficient for high-quality perception. Unlike `Shortest path`, which lacks the capacity

Table 4. Ablation study on reward functions. Visual grounding is evaluated by mAP, segmentation by IoU and Dice, and 3D box estimation by IoU and Center Score (higher is better). Degraded results are highlighted in red, while improved results are highlighted in green.

Reward function	Visual Grounding			Segmentation		3D Box Estimation	
	mAP@0.5 ↑	mAP@0.75 ↑	mAP _{avg} ↑	IoU ↑	Dice ↑	IoU ↑	Center Score ↑
Format	—	—	—	—	—	—	—
Format + Geometric	0.8292 (+4.20%)	0.6872 (+10.39%)	0.7582 (+6.91%)	0.5942 (+5.71%)	0.6667 (+4.20%)	0.2905 (+9.71%)	0.6125 (+11.38%)
Format + Confidence	0.7115 (-10.60%)	0.5562 (-10.65%)	0.6339 (-10.62%)	0.5253 (-6.54%)	0.5973 (-6.64%)	0.2902 (+9.59%)	0.5954 (+8.27%)
Format + Confidence + Geometric	0.8627 (+8.40%)	0.7055 (+13.33%)	0.7841 (+10.56%)	0.6251 (+11.21%)	0.7002 (+9.44%)	0.3195 (+20.67%)	0.6600 (+20.03%)

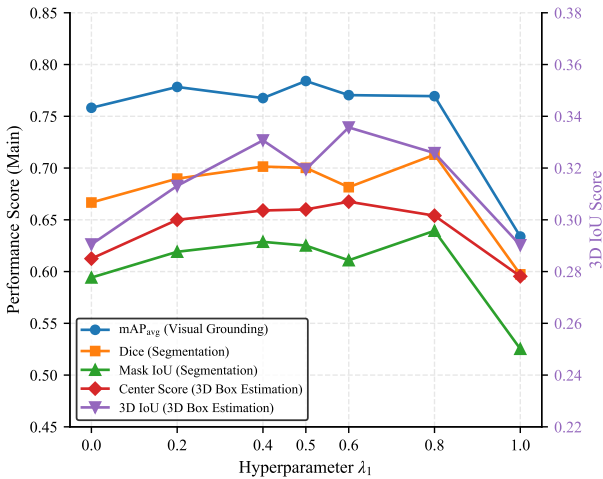


Figure 7. Impact of hyperparameter λ_1 on different tasks. The left y-axis corresponds to Grounding and Segmentation metrics, while the right y-axis highlights the 3D IoU performance.

for viewpoint-level planning, Sea² strategically optimizes the camera pose to mitigate occlusion and maximize visual informativeness.

Finally, directly prompting a compact VLM controller

without task-aligned training underperforms the static initial value on all metrics, highlighting that naively using a VLM as a policy is insufficient; embodiment alignment and reward-driven refinement are necessary.

We further evaluate Sea² on HM3D, a dataset featuring more complex and high-fidelity 3D-scanned reconstructions of real-world environments. As summarized in Table 2, the performance gains on HM3D mirror those observed on ReplicaCAD, reinforcing the effectiveness and robustness of our active perception strategy across diverse scene distributions.

4.3. Ablation Study

Training Strategy. Table 3 compares *RL-Only*, *SFT-Only*, and our *SFT+RL*. Training the policy from scratch with RL

is unstable and underperforms the initial value on recognition metrics. SFT on rule-based trajectories yields consistent gains across tasks, validating the importance of a spatially grounded cold start. The full *SFT+RL* pipeline achieves the best results on all metrics, showing that SFT provides stable priors while RL unlocks task-specific view selection beyond heuristic behaviors.

Reward Design. Table 4 further disentangles the contribution of each reward term in Equation (2). Using *confidence* alone (*Format+Confidence*) is unstable: it degrades visual grounding and segmentation, while offering improvements only on 3D box estimation. Although confidence is a strong directional signal toward better viewpoints, it is also noisy and volatile; the effect is most pronounced in VG, where the signal comes solely from GroundingDINO, making the policy more susceptible to detector-specific jitter. By contrast, the *geometric* term (*Format+Geometric*) is stable and module-agnostic. Optimizing area/center alignment (Equation (6)) yields consistent but limited improvements across tasks, reflecting that geometric shaping provides reliable spatial guidance yet lacks model/task specificity. Crucially, combining the two signals (*Format+Confidence+Geometric*) produces large and uniform gains. Geometry supplies smooth, low-variance spatial shaping, while confidence calibrates view selection to the current frozen module and task, turning a noisy-but-informative signal into a robust control objective. Figure 7 analyzes the impact of λ_1 , indicating a necessary trade-off between the reward components. Consequently, we fix $\lambda_1 = 0.5$ for all main evaluations.

5. Conclusions

We presented our Sea² that adapts pre-trained perception modules to new embodied environments without updating parameters or requiring downstream labels. By learning a pose-control policy through supervised heuristic trajectories and unsupervised GRPO-based RL, the agent actively selects informative viewpoints using only scalar feedback from frozen perception modules. Experiments on visual

grounding, segmentation, and 3D box estimation demonstrate gains, 13.54%, 15.92%, and 27.68% respectively on ReplicaCAD, highlighting that intelligently controlling viewpoints offers an efficient and annotation-free alternative to traditional model fine-tuning for domain adaptation.

References

- Ammirato, P., Poirson, P., Park, E., Košecká, J., and Berg, A. C. A dataset for developing and benchmarking active vision. In *2017 IEEE international conference on robotics and automation (ICRA)*, pp. 1378–1385. IEEE, 2017.
- Ao, S., Salim, F. D., and Khan, S. Emac+: Embodied multimodal agent for collaborative planning with vlm+llm, 2025. URL <https://arxiv.org/abs/2505.19905>.
- Bai, S., Chen, K., Liu, X., Wang, J., Ge, W., Song, S., Dang, K., Wang, P., Wang, S., Tang, J., et al. Qwen2. 5-vl technical report. *arXiv preprint arXiv:2502.13923*, 2025.
- Chaplot, D. S., Dalal, M., Gupta, S., Malik, J., and Salakhutdinov, R. R. Seal: Self-supervised embodied active learning using exploration and 3d consistency. *Advances in neural information processing systems*, 34:13086–13098, 2021.
- Cheng, T., Song, L., Ge, Y., Liu, W., Wang, X., and Shan, Y. Yolo-world: Real-time open-vocabulary object detection. In *2024 IEEE/CVF Conference on Computer Vision and Pattern Recognition (CVPR)*, pp. 16901–16911, 2024. doi: 10.1109/CVPR52733.2024.01599.
- Di Giammarino, L., Sun, B., Grisetti, G., Pollefeys, M., Blum, H., and Barath, D. Learning where to look: Self-supervised viewpoint selection for active localization using geometrical information. In *European Conference on Computer Vision*, pp. 188–205. Springer, 2024.
- Ding, W., Majcherczyk, N., Deshpande, M., Qi, X., Zhao, D., Madhivanan, R., and Sen, A. Learning to view: Decision transformers for active object detection. *arXiv preprint arXiv:2301.09544*, 2023.
- Fan, L., Liang, M., Li, Y., Hua, G., and Wu, Y. Evidential active recognition: Intelligent and prudent open-world embodied perception. In *Proceedings of the IEEE/CVF Conference on Computer Vision and Pattern Recognition*, pp. 16351–16361, 2024.
- Fang, Z., Jain, A., Sarch, G., Harley, A. W., and Fragkiadaki, K. Move to see better: Self-improving embodied object detection. *arXiv preprint arXiv:2012.00057*, 2020.
- He, K., Chen, X., Xie, S., Li, Y., Dollár, P., and Girshick, R. B. Masked autoencoders are scalable vision learners. *2022 IEEE/CVF Conference on Computer Vision and Pattern Recognition (CVPR)*, pp. 15979–15988, 2021. URL <https://api.semanticscholar.org/CorpusID:243985980>.
- Jiang, B., Chen, S., Zhang, Q., Liu, W., and Wang, X. Alphadrive: Unleashing the power of vlms in autonomous driving via reinforcement learning and reasoning. *arXiv preprint arXiv:2503.07608*, 2025.
- Jing, Y. and Kong, T. Learning to explore informative trajectories and samples for embodied perception. *arXiv preprint arXiv:2303.10936*, 2023.
- Kirillov, A., Mintun, E., Ravi, N., Mao, H., Rolland, C., Gustafson, L., Xiao, T., Whitehead, S., Berg, A. C., Lo, W.-Y., Dollár, P., and Girshick, R. Segment anything, 2023. URL <https://arxiv.org/abs/2304.02643>.
- Kotar, K. and Mottaghi, R. Interactron: Embodied adaptive object detection. In *Proceedings of the IEEE/CVF conference on computer vision and pattern recognition*, pp. 14860–14869, 2022.
- Li, J., Li, D., Savarese, S., and Hoi, S. Blip-2: Bootstrapping language-image pre-training with frozen image encoders and large language models. In *International conference on machine learning*, pp. 19730–19742. PMLR, 2023.
- Lin, T.-Y., Maire, M., Belongie, S., Bourdev, L., Girshick, R., Hays, J., Perona, P., Ramanan, D., Zitnick, C. L., and Dollár, P. Microsoft coco: Common objects in context, 2015. URL <https://arxiv.org/abs/1405.0312>.
- Liu, H., Li, C., Wu, Q., and Lee, Y. J. Visual instruction tuning. *Advances in neural information processing systems*, 36:34892–34916, 2023.
- Liu, S., Zeng, Z., Ren, T., Li, F., Zhang, H., Yang, J., Jiang, Q., Li, C., Yang, J., Su, H., Zhu, J., and Zhang, L. Grounding dino: Marrying dino with grounded pre-training for open-set object detection, 2024. URL <https://arxiv.org/abs/2303.05499>.
- Ouyang, L., Wu, J., Jiang, X., Almeida, D., Wainwright, C., Mishkin, P., Zhang, C., Agarwal, S., Slama, K., Ray, A., et al. Training language models to follow instructions with human feedback. *Advances in neural information processing systems*, 35:27730–27744, 2022.
- Radford, A., Kim, J. W., Hallacy, C., Ramesh, A., Goh, G., Agarwal, S., Sastry, G., Askell, A., Mishkin, P., Clark, J., et al. Learning transferable visual models from natural language supervision. In *International conference on machine learning*, pp. 8748–8763. PmlR, 2021.

- Rafailov, R., Sharma, A., Mitchell, E., Manning, C. D., Ermon, S., and Finn, C. Direct preference optimization: Your language model is secretly a reward model. *Advances in neural information processing systems*, 36: 53728–53741, 2023.
- Ramakrishnan, S. K., Gokaslan, A., Wijmans, E., Maksymets, O., Clegg, A., Turner, J. M., Undersander, E., Galuba, W., Westbury, A., Chang, A. X., Savva, M., Zhao, Y., and Batra, D. Habitat-matterport 3d dataset (HM3d): 1000 large-scale 3d environments for embodied AI. In *Thirty-fifth Conference on Neural Information Processing Systems Datasets and Benchmarks Track (Round 2)*, 2021. URL <https://openreview.net/forum?id=-v4OuqNs5P>.
- Ravi, N., Gabeur, V., Hu, Y.-T., Hu, R., Ryali, C., Ma, T., Khedr, H., Rädle, R., Rolland, C., Gustafson, L., et al. Sam 2: Segment anything in images and videos. *arXiv preprint arXiv:2408.00714*, 2024.
- Ren, T., Liu, S., Zeng, A., Lin, J., Li, K., Cao, H., Chen, J., Huang, X., Chen, Y., Yan, F., Zeng, Z., Zhang, H., Li, F., Yang, J., Li, H., Jiang, Q., and Zhang, L. Grounded sam: Assembling open-world models for diverse visual tasks, 2024. URL <https://arxiv.org/abs/2401.14159>.
- Savva, M., Kadian, A., Maksymets, O., Zhao, Y., Wijmans, E., Jain, B., Straub, J., Liu, J., Koltun, V., Malik, J., et al. Habitat: A platform for embodied ai research. In *Proceedings of the IEEE/CVF international conference on computer vision*, pp. 9339–9347, 2019.
- Scarpellini, G., Rosa, S., Morerio, P., Natale, L., and Del Bue, A. Look around and learn: Self-training object detection by exploration. In *European Conference on Computer Vision*, pp. 72–88. Springer, 2024.
- Shao, Z., Wang, P., Zhu, Q., Xu, R., Song, J., Bi, X., Zhang, H., Zhang, M., Li, Y., Wu, Y., et al. Deepseekmath: Pushing the limits of mathematical reasoning in open language models. *arXiv preprint arXiv:2402.03300*, 2024.
- Shi, X., Qiao, Y., Liu, L., and Dayoub, F. Embodied domain adaptation for object detection. *arXiv preprint arXiv:2506.21860*, 2025.
- Szot, A., Clegg, A., Undersander, E., Wijmans, E., Zhao, Y., Turner, J., Maestre, N., Mukadam, M., Chaplot, D. S., Maksymets, O., et al. Habitat 2.0: Training home assistants to rearrange their habitat. *Advances in neural information processing systems*, 34:251–266, 2021.
- Wang, W., Gao, Z., Gu, L., Pu, H., Cui, L., Wei, X., Liu, Z., Jing, L., Ye, S., Shao, J., et al. Internvl3. 5: Advancing open-source multimodal models in versatility, reasoning, and efficiency. *arXiv preprint arXiv:2508.18265*, 2025.
- Xiao, B., Wu, H., Xu, W., Dai, X., Hu, H., Lu, Y., Zeng, M., Liu, C., and Yuan, L. Florence-2: Advancing a unified representation for a variety of vision tasks. In *Proceedings of the IEEE/CVF Conference on Computer Vision and Pattern Recognition*, pp. 4818–4829, 2024.
- Xiao, L., Yang, X., Peng, F., Yan, M., Wang, Y., and Xu, C. Clip-vg: Self-paced curriculum adapting of clip for visual grounding. *IEEE Transactions on Multimedia*, 26: 4334–4347, 2023.
- Yang, A., Li, A., Yang, B., Zhang, B., Hui, B., Zheng, B., Yu, B., Gao, C., Huang, C., Lv, C., et al. Qwen3 technical report. *arXiv preprint arXiv:2505.09388*, 2025.
- Yang, J., Ren, Z., Xu, M., Chen, X., Crandall, D. J., Parikh, D., and Batra, D. Embodied amodal recognition: Learning to move to perceive objects. In *Proceedings of the IEEE/CVF International Conference on Computer Vision*, pp. 2040–2050, 2019.
- Yin, H., Xu, X., Wu, Z., Zhou, J., and Lu, J. Sg-nav: Online 3d scene graph prompting for llm-based zero-shot object navigation, 2024. URL <https://arxiv.org/abs/2410.08189>.
- Yu, Q., Zhang, Z., Zhu, R., Yuan, Y., Zuo, X., Yue, Y., Dai, W., Fan, T., Liu, G., Liu, L., et al. Dapo: An open-source llm reinforcement learning system at scale. *arXiv preprint arXiv:2503.14476*, 2025.
- Zeng, R., Wen, Y., Zhao, W., and Liu, Y.-J. View planning in robot active vision: A survey of systems, algorithms, and applications. *Computational Visual Media*, 6(3):225–245, 2020.
- Zhang, J., Wang, K., Wang, S., Li, M., Liu, H., Wei, S., Wang, Z., Zhang, Z., and Wang, H. Uni-navid: A video-based vision-language-action model for unifying embodied navigation tasks. *arXiv preprint arXiv:2412.06224*, 2024a.
- Zhang, J., Wang, K., Xu, R., Zhou, G., Hong, Y., Fang, X., Wu, Q., Zhang, Z., and Wang, H. Navid: Video-based vlm plans the next step for vision-and-language navigation. *arXiv preprint arXiv:2402.15852*, 2024b.
- Zhang, L., Hao, X., Xu, Q., Zhang, Q., Zhang, X., Wang, P., Zhang, J., Wang, Z., Zhang, S., and Xu, R. MapNav: A Novel Memory Representation via Annotated Semantic Maps for Vision-and-Language Navigation. *arXiv e-prints*, art. arXiv:2502.13451, February 2025. doi: 10.48550/arXiv.2502.13451.
- Zheng, C., Liu, S., Li, M., Chen, X.-H., Yu, B., Gao, C., Dang, K., Liu, Y., Men, R., Yang, A., et al. Group sequence policy optimization. *arXiv preprint arXiv:2507.18071*, 2025.